High Speed Tensile Performance and Fractography of Acrylic Latex Films

SARAH T. ECKERSLEY,[1] ALAN PLUMTREE,[2] and ALFRED RUDIN[3,*]

Institute for Polymer Research: [1]Department of Chemical Engineering, [2]Department of Mechanical Engineering, [3]Department of Chemistry, University of Waterloo, Waterloo, Ontario, Canada N2L 3G1

SYNOPSIS

The performance of acrylic (50 : 50 MMA/BuA) latexes was investigated as a function of fusion level using high speed tensile testing. The structure of the copolymer was varied via the addition of molecular weight modifiers to the emulsion polymerizations. Chain transfer agent (CBr_4) was used to reduce the copolymer modulus, and crosslinker (EGDM, ethylene glycol dimethacrylate) was added to increase the modulus. The resulting materials exhibited a wide range of viscoelastic behavior (G^* varied from $\sim 10^7$ dyne cm^{-2} to $\sim 10^9$ dyne cm^{-2}). Fracture energy and peak force at break were measured as a function of the complex modulus. It was found that both of these parameters showed a maximum with respect to G^* that corresponded to intermediate levels of crosslinking. This observation was explained in terms of the degree of coalescence of the films. Fully fused films (excess CBr_4) were brittle and performed poorly, conceivably because of insufficient entanglement to support stress. Marginally fused films also exhibited inferior, brittle behavior. The films cast from latexes synthesized with low levels of molecular weight modifiers showed intermediate fusion levels and superior tensile performance. The quantitative results were rationalized using scanning electron microscopy (SEM) of both the virgin films and the fracture surfaces. For comparison, the same materials were tested in a fully fused state following hot pressing. The behavior paralleled that expected for vulcanized rubbers in which lightly crosslinked materials exhibit the highest tensile strength. © 1993 John Wiley & Sons, Inc.

INTRODUCTION

In a coating film, there are two main parameters that will control the performance with respect to strength and durability. The mechanical properties of the bulk polymer will decide the ultimate properties of the film or coating. However, the film will reflect the bulk properties of the polymer only under conditions where the latex particles are completely coalesced and diffusion of the polymer molecules across the interparticle boundaries has occurred. In other words, the film will display the properties of the bulk material when and if the film becomes homogeneous.

Because the polymer material properties as well as the degree of film fusion would affect film performance, it was decided to use mechanical testing, along with scanning electron microscopy (SEM), to study the fusion behavior of a series of poly(methyl methacrylate-*co*-butyl acrylate) latexes having varying physical properties. The physical properties were adjusted by incorporating molecular weight modifiers (ethylene glycol dimethacrylate crosslinking agent and CBr_4 chain transfer agent) into the emulsion polymerization recipes.

The fracture surfaces of the specimens were also examined using SEM. Fractography has had only limited application in the field of polymer materials science. Previous work has concentrated on composites, blends, and glassy thermoplastics. Doll can be consulted for an exhaustive review of the fractography of amorphous (primarily glassy) thermoplastics.[1]

It is possible to use a variety of mechanical tests to evaluate a polymer. Each of these techniques yields unique information. Consequently, the test

* To whom correspondence should be addressed.

Journal of Applied Polymer Science, Vol. 48, 1689–1700 (1993)
© 1993 John Wiley & Sons, Inc. CCC 0021-8995/93/101689-12

method appropriate to the information sought should be selected. There were two obvious choices for studying the latex films: low and high speed tensile testing. The low speed tensile test would provide insight into the performance of the coating under typical usage stresses such as scrubbing, blistering, and peeling. A latex film is not likely to encounter the stresses mimicked by high speed tests under ordinary use. However, the high speed tensile test has a distinct advantage for investigating the mechanical properties as a function of degree of fusion. The polymer specimens tend to undergo brittle fracture at very high strain rates ($\sim$ 1 m s^{-1}). Therefore, under brittle fracture conditions, it can be postulated that the films will fail in the partially fused interstitial regions. Consequently, high speed tensile testing was the technique chosen. This technique has been employed by several researchers to study the toughness of impact modified thermoplastics[2] and elastomers.[3] A similar tensile impact test has been employed to investigate the properties of glassy thermoplastics[4] and impact modified thermoplastics.[5]

The mechanical behavior of the polymers was compared in the cast film and the fully fused state. This was accomplished by preparing two sets of specimens. In the first, the latex films were simply dried and then tested, providing samples in their "natural" state of coalescence. For comparison, the second set of specimens was prepared by pressing the samples at elevated temperature.

In most commercial water-based coating materials, the latex becomes fully fused only after the completion of a process termed "further gradual coalescence" or autohesion.[6] As the film ages, it is postulated that the polymer chain ends or looped segments of chains diffuse across the interparticle boundaries. Recent work utilizing small angle neutron scattering (SANS)[7-11] and molecular energy transfer fluorescence techniques[12] have shown that the diffusion process is responsible for the ultimate film properties. At a given temperature, the duration of this process (if it occurs at all) is a function of the nature of the polymer, the molecular weight, and the degree of crosslinking.

Table I Surfactant Free Emulsion Polymerization

Reactor charge	
Deionized water	210 *g*
Ammonium persulphate initiator	1.35 *g*
Monomer mixture	
Butyl acrylate	101.4 *g*
Methyl methacrylate	101.4 *g*
Methacrylic acid	2.55 *g*
Molecular weight modifier	*x g*

Table II Emulsion Polymer Molecular Weight Modifiers and Particle Size Distributions

Latex	Modifier	Mass Modifier *x* (*g*)	D_n (nm)	D_w/D_n
L1	CBr_4	5.00	671	1.010
L2	CBr_4	2.50	680	1.030
L3	CBr_4	0.20	647	1.009
L4	—	—	580	1.010
L5	EGDM[a]	3.00	699	1.010
L6	EGDM[a]	8.00	899	1.007
L7	EGDM[a]	12.00	984	1.006

[a] Ethylene glycol dimethacrylate.

EXPERIMENTAL

Emulsion Polymerization

Latexes were synthesized using a semi-continuous reaction scheme. The proportions of all reactants, except for the molecular weight modifiers, were kept constant between the various recipes. The basic emulsion polymerization recipe is given in Table I. Table II provides information about the molecular weight modifiers used, and the resulting particle size and particle size distributions.

All reactions were carried out in a 1 L kettle reactor equipped with an overhead condenser and a jacketed mechanical stirrer. The stirring rate was maintained at 250 rpm throughout the reaction.

The water and initiator were charged to the reactor and maintained at a temperature of 80°C with continuous stirring. The monomer mixture was fed to the reactor via a fluid metering pump at a constant rate of approximately 1 mL min^{-1}. No monomer accumulation was observed at any time. Therefore, it was assumed that reaction was starve-fed and that the composition of the terpolymer was uniform throughout the latex particle. When monomer addition was complete, the reaction was continued for 1 h. The latex was then gradually cooled to ambient temperature. Finally, the latex was filtered through a 100-mesh screen to remove the minimal amount of grit formed during the polymerization.

Latex particle size measurements were obtained using an ICI-Joyce Loebl Disk Centrifuge according to a method described elsewhere.[13] Unfortunately, the significant gel content of most of the polymers prohibited the measurement of molecular weights by size exclusion chromatography. Attempts were

made to determine the gel fraction by Soxhlet solvent extraction. The results were not reliable, however, because of poor reproducibility.

Sample Preparation

Specimens to be tested at the natural fusion level of the polymer latex films were prepared by casting the latex on PTFE sheets. These samples will be referred to as the virgin films. The second set of specimens were completely fused by pressing at elevated temperature and pressure several times. The conditions were selected for each individual material, since the viscoelastic properties varied widely. Typical conditions ranged from $T = 100°C$, $P = 110$ kPa (polymer L1) to $T = 100°C$, $P = 393$ kPa (polymer L7). These specimens will be referred to as treated films.

Following preparation of the polymer films, unnotched dogbone specimens were obtained. Unnotched specimens do not yield data as reproducible as their notched counterparts. However, all the samples could not be notched, because of the brittle character of many of the materials. The dogbone specimens were cut directly from the polymer sheets using a preheated die. Preheating was required, again because of the brittle nature of the materials at room temperature. The cross sections of the specimens were typically 2 mm × 5 mm. The gauge length of the specimen was 20 mm. The width was measured in five places along the length of the specimen, then averaged. Measurement of the specimen at the exact point of breakage was prohibited because of sample necking.

Data Acquisition and Analysis

A pneumatically driven high speed tensile device was designed and built at the University of Waterloo by J. Pronovost and D. Cook.[14] The piston was equipped with a hydraulic speed regulator allowing velocities of up to 1 m s^{-1} to be controlled.

The apparatus was interfaced with a Rapid Systems R4004 A/D board. Two channels were used. Position information was supplied via a linear displacement transducer. The other channel was connected to a PCB load cell. Data were collected at a frequency of one datum every 40 μs for both channels. All tests were performed at room temperature.

Dynamic Mechanical Temperature Sweeps

Measurements of the polymer moduli were made using a Rheometrics Model 605 mechanical spectrometer. Both torsion rectangular and parallel plate geometries were employed. In the case of the parallel plate geometry, 8 mm diameter and 25 mm diameter plates were used.

The initial strain experienced by the sample was chosen by preliminary experiments. Strain sweeps were performed at the lowest temperature in the experimental range and the highest frequency of those selected. Strain sweeps were performed to determine an initial strain value that fulfilled several criteria. Most importantly, the torque on the transducer had to be within the safe operating limits of the machine (this sets an upper limit for the strain). Also, the measurement of tan delta had to be within the measuring capabilities of the Rheometrics (this sets a lower limit for the strain). Finally, to allow comparison of the materials at different deformations and different geometries, it was necessary that the polymer behave in a linear viscoelastic manner at the strain chosen.

For all experiments, forced oscillation measurements were obtained at three frequencies for each temperature in the temperature sweep experiments. At the lower end of the selected temperature range, torsion rectangular geometry was used because of the stiffness of the polymers. When the torque became unacceptably low, the torsion rectangular geometry was exchanged for the small parallel plate geometry. At the higher temperatures, the larger parallel plates were required. For all geometries, as the signal diminished with increasing sample temperature, the percent strain experienced by the specimen was increased. This procedure is only acceptable in the linear viscoelastic strain region, where the dynamic mechanical response of the material is not a function of the degree of deformation. Linear viscoelasticity was confirmed by performing a strain sweep at the terminal experimental temperature for each geometry. As for the low temperature strain sweep, the test was done at the highest frequency used in the temperature sweep.

SEM

The surfaces of the cast latex films and specimen fracture surfaces were examined by SEM. All specimens were gold sputtered to prevent charging and distortion of the specimens in the electron beam.

RESULTS AND DISCUSSION

Fracture Energy

Generally, the latex films studied displayed both ductile and brittle failure. However, only the poorest

of the virgin films, (L1) and (L7), exhibited purely brittle failure. These materials were synthesized with the highest proportion of chain transfer agent and crosslinker respectively. Figures 1 and 2 are representative of the raw data obtained for two specimens of film (L5) that failed by both mechanisms. The abscissa corresponds to force, and the ordinate to extension. Figure 1 shows a sample that broke during elastic loading. Figure 2 depicts the same sample yielding, and then drawing before failure. Note that the ordinate scales are different for the two figures. The extension at break for the ductile failure (Fig. 2) was approximately ten times greater than for the brittle failure (Fig. 1).

Generally, the same behavior was observed for the specimens that had been prepared from pressure and temperature treated films. All the samples (again with the exceptions of L1 and L7) failed by both mechanisms. However, the energy to break was up to an order of magnitude higher than for the virgin films.

It is expected that a particular sample will fail in either a brittle or a ductile manner, reflecting the viscoelastic character of the polymer. The fact that only a fraction of samples of a given polymer was brittle is probably due to imperfections in the polymer films. Because of the nature of emulsion polymerization, all latex polymers contain impurities. For example, the films contain residual salts resulting from the thermal decomposition of the initiator molecules. Thus, it is likely that some of the samples failed prematurely because of these imperfections. These data were not discounted, since the results were consistent with those for ductile failure. In addition, the ultimate force at break is a material

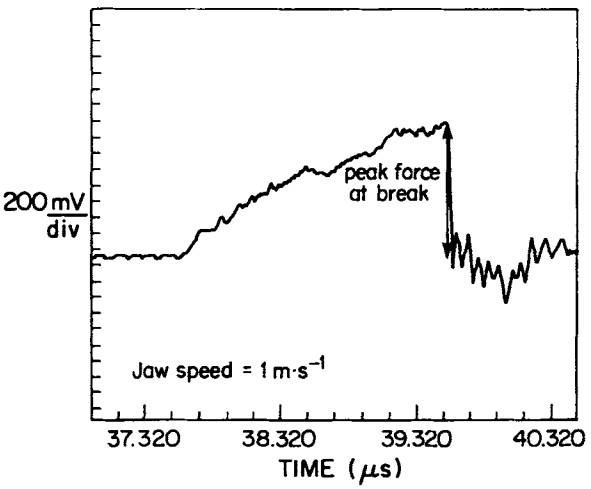

Figure 1 Brittle failure (Film L5).

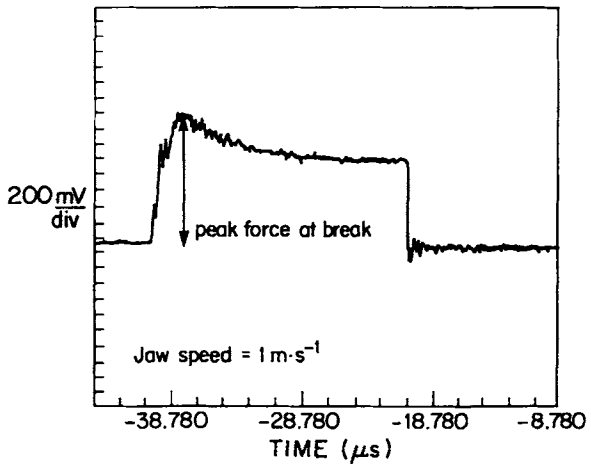

Figure 2 Ductile failure (Film L5).

property but is dependent on the presence of defects. Figure 3 shows the energies to break, E_b (measured in J mm^{-2}) as a function of the complex moduli of the materials. The complex modulus of a material reflects its rigidity. Figure 4 shows the complex moduli of the emulsion polymers as a function of temperature obtained from dynamic mechanical analysis at a frequency of 0.1 rad s^{-1}. As expected, since the polymers are virtually all chemically identical, the materials exhibit identical behaviour in the glassy region (i.e., $T <$ approximately 5°C). The differences in the viscoelastic nature of the copolymers is most apparent in the rubbery region ($T > \sim 50$°C). The polymer prepared with the highest concentration of chain transfer agent (L1) does not actually exhibit rubbery behaviour. The curve decays as for a viscous liquid. Conversely, the materials synthesized with crosslinking agents show rubbery plateaux. The addition of chain transfer agent evidently has a more dramatic effect on the viscoelastic behaviour of the copolymer. The effect of variations in the crosslinker concentration is less apparent since the unmodified recipe yielded polymers that contained gel resulting from chain transfer to polymer during the polymerization.

The films prepared for this study were dried at room temperature (T = 22°C). This temperature falls in the glass to rubber transition region for all the materials investigated. It would be expected that all of the moduli would increase as the molecular weight modifier is adjusted from L1 to L7. However, experimental uncertainty will be most evident in the transition region where the decrease in modulus with temperature is greatest. Hence, the modulus temperature curves do not exactly follow the pattern predicted. Nevertheless, the results described below

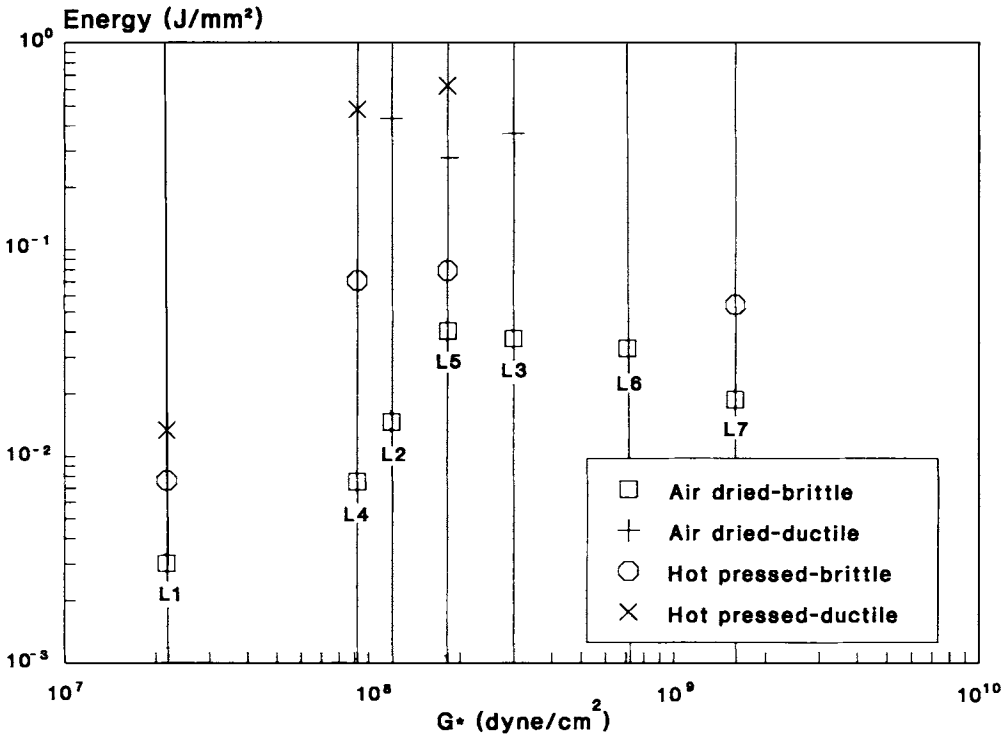

Figure 3 Energy to break as a function of modulus for latex films.

demonstrate that the fracture behaviour of the polymers corresponds to the measured values of the modulus.

Generally, Figure 3 shows an increase in E_b as a function of G^* to a maximum, then a decrease. The low energy to break for the virgin film cast from

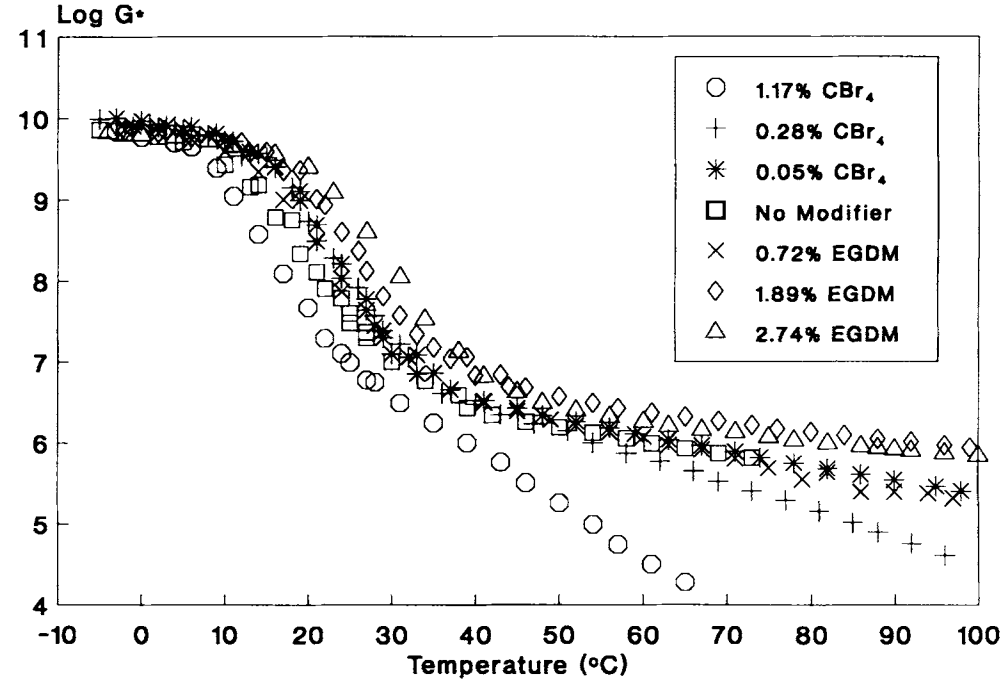

Figure 4 Modulus as a function of temperature.

latex L1 is attributed to the inferior quality of the polymer itself, rather than any effects resulting from the film fusion level. Figure 5 gives a series of scanning electron micrographs revealing that films cast from latexes L1 and L2 were completely fused within the 24-h period that the films are allowed to dry before exposure to the SEM's high vacuum. This can be deduced from the lack of any residual spherical structure remaining from the original latex particles. Since L1 is completely fused in all tests, the poor performance is simply caused by the high concentration of CBr_4 employed in the emulsion poly-

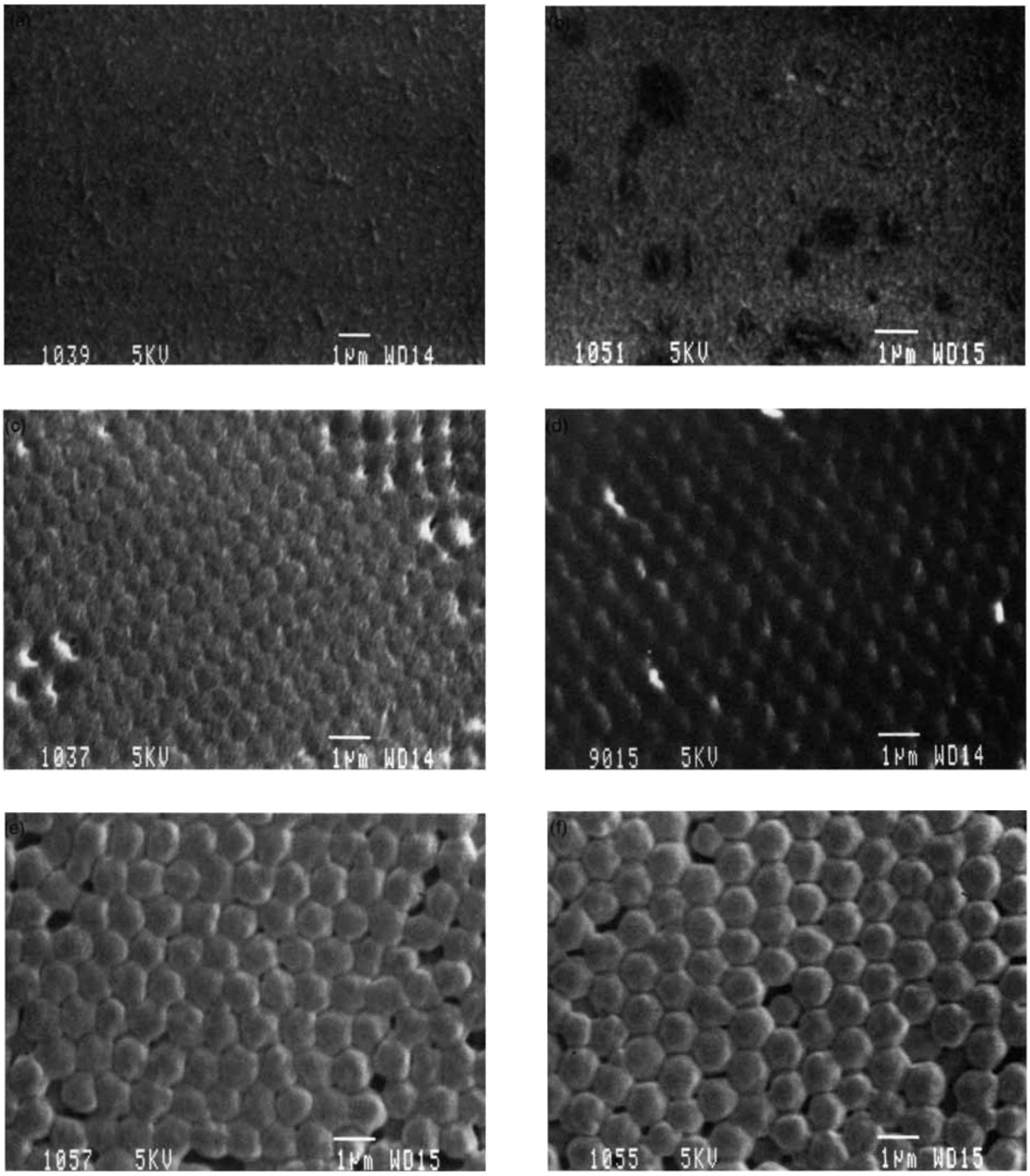

Figure 5 Scanning electron micrographs of virgin films. (a) Virgin film, latex L1; (b) virgin film, latex L2; (c) virgin film, latex L4; (d) virgin film, latex L5; (e) virgin film, latex L6; (f) virgin film, latex L7.

merization that results in low molecular weight material. The slight improvement seen after hot pressing is attributed to further consolidation of the original particles. Although the films appear to be fully fused after only 24 h, chain end diffusion will still occur slowly over time or rapidly at elevated temperature and pressure. The resulting homogeneity likely accounts for the improved performance. In the case of chain transfer agent modified polymers, it is postulated that the level of entanglement is insufficient to impart good mechanical properties to the material. This is in agreement with the work of Bersted,[15] relating tensile impact strength to entanglement density. Molecular weights were not measured for any of the polymers, since this is not experimentally feasible for polymers with appreciable gel contents (i.e., most of the materials synthesized).

Although the films prepared from latex L7 failed in a brittle manner, the failure mechanism was different because the high concentration of crosslinking agent used in the emulsion reaction prevents virtually any fusion of the film, as shown in Figure 5(f). The film contains obvious structural imperfections that are natural sites for crack formation.

In the virgin state, the remainder of the materials show behavior intermediate between L1 and L7, as illustrated in Figure 3. Apparently, two processes counteract one another. As the molecular weight and crosslink density of the material are increased, so is the strength of the bulk material. However, increasing crosslink density hinders coalescence of the latex particles, resulting in physical imperfections, and consequently, poor response to stress. Therefore, there is an optimum range corresponding to intermediate levels of molecular weight modifiers. Note that with the exception of L1, the fracture energies of the samples that exhibited ductile failure are essentially equivalent.

Figure 3 also shows the energy to break as a function of the modulus for treated films. The same trends are observed as for the virgin films. There is an optimum modulus range corresponding to a range of emulsion formulations. In general, the results are in accordance with the work of Bueche and Dudek[16] on the tensile strength of rubbers at $T \gg T_g$ and relatively slow elongation rates. These conditions correspond to conditions far from the glassy state. These authors proposed that the superior performance of lightly crosslinked rubbers could be attributed to the high fraction of chains in a fully extended state at the instant of fracture. That is, in a highly crosslinked system, the chains can extend to a much lesser degree before catastrophic failure because of restriction by the crosslink junctions.

Peak Force at Break

In addition to energy to break, peak force was also measured. This is the maximum stress experienced by the sample prior to failure (by either mechanism) as indicated in the raw data curves (Figs. 1 and 2). The peak force is independent of the failure mechanism, and is an alternate means of comparing the performance of the films. Figure 6 shows the peak force as a function of the complex modulus. The trend is similar to that seen in Figure 3. The sample containing an excess of chain transfer agent (L1) performs poorly. At the other extreme, the sample containing an excess of crosslinking agent (L7) also fractures easily. Polymers synthesized with intermediate levels of molecular weight modifiers exhibit the highest peak force. This is particularly evident for the fused films.

Fractography

The differences in fracture energies can be explained in terms of the fusion behavior of the films. The SEM micrographs in Figures 7–10 show the fracture surfaces of the virgin films. Figure 7 depicts the micrographs obtained from the fracture surface of the film cast from latex L1. The micrographs are typical of a brittle fracture. A general view of the fracture surface is shown in Figure 7(a), indicating crack initiation on slightly different planes, as illustrated by the contours radiating from the initiation point (at bottom of picture). These contours are shown at a higher magnification in Figure 7(b). This is the same field shown in Figure 7(a). As crack propagation continues, the crack levels merge, resulting in a lower energy crack travelling at a faster rate. The corresponding monoplanar fracture surface is shown in Figure 7(c). This surface is virtually identical to the 'as cast' film surface seen in Figure 5(a), suggesting that the microstructure of the material is uniform throughout the specimen. The homogeneous, monoplanar brittle crack corresponds to the low energy to break measured experimentally.

The primary fracture mechanism is brittle failure. However, a secondary mechanism may occur. Close examination of Figure 7(b) and (c) reveals microvoids $\sim 0.1\ \mu m$ in diameter. These are certainly not due to the removal of latex particles. The microvoids are likely created when impurities such as salt crystals or dust are dislodged during crack formation.

Films cast from L7 were also brittle, though the failure mechanism was different. Figure 8 shows a fracture surface of film L7. An overview of the crack is shown in Figure 8(a), propagating from top to bottom of the picture. As with the other highly brittle

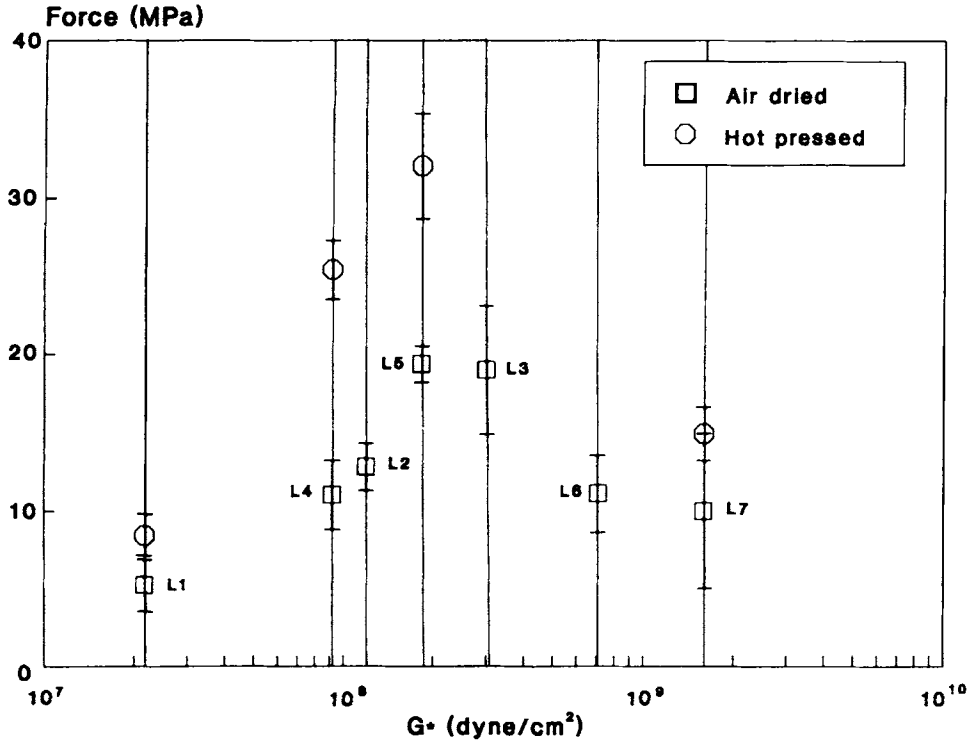

Figure 6 Peak force at break as a function of modulus.

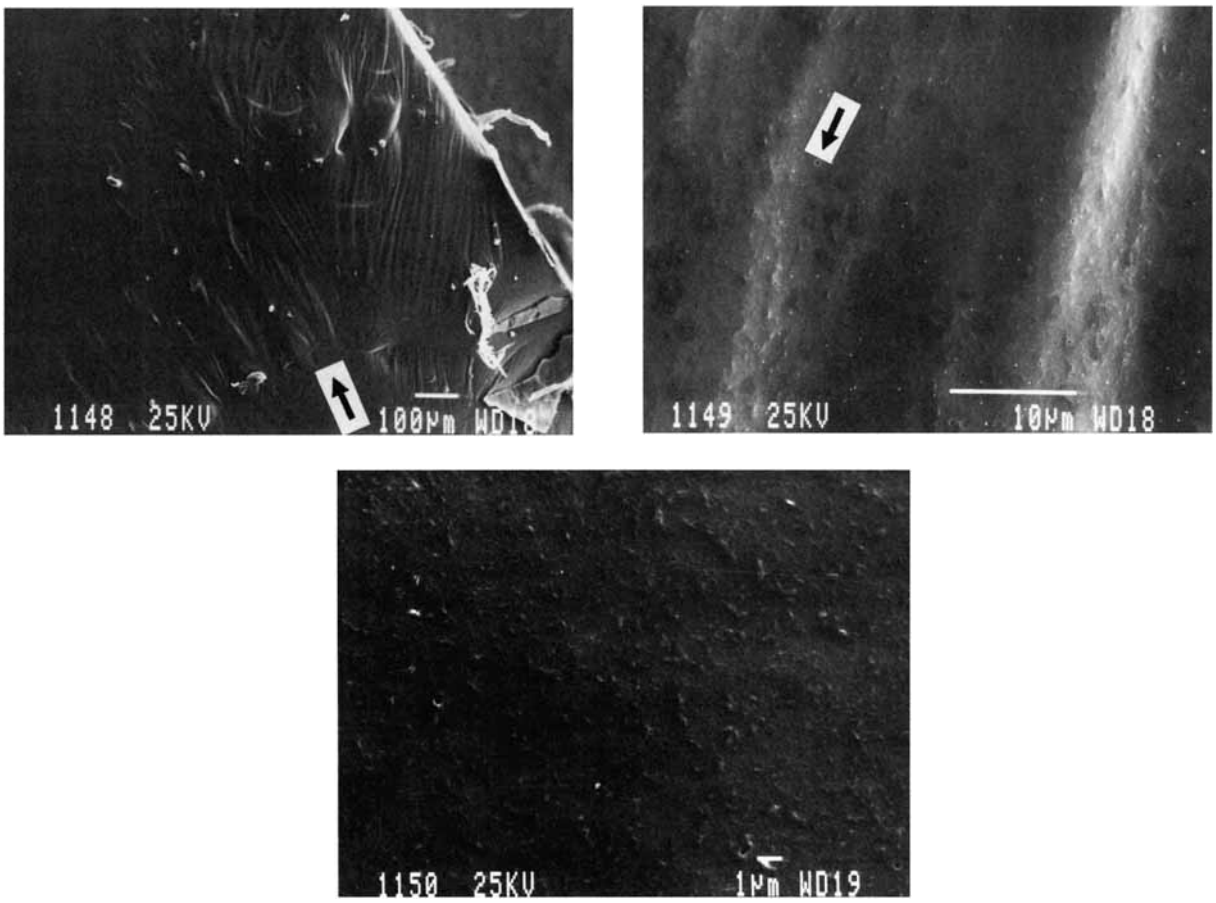

Figure 7 Scanning electron micrographs of fracture surface, Film L1.

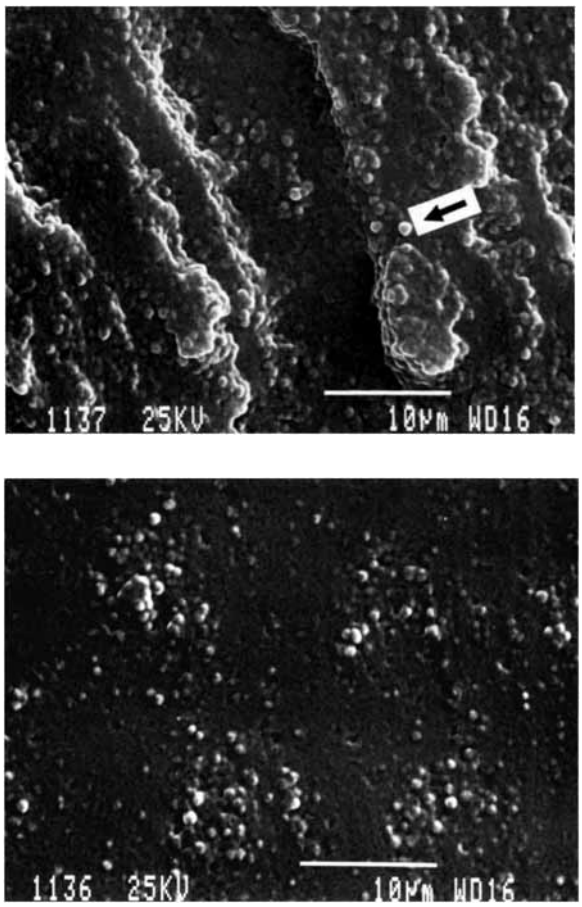

Figure 8 Scanning electron micrographs of fracture surface, Film L7.

material (L1), the crack initially travels on different planes, as shown in Figure 8(a) and (b). Further from the initiation point, the crack fronts combine and monoplanar failure continues, as depicted in Figure 8(c). The energies required to create these surfaces are of the same order of magnitude for both L1 and L7. However, on a microscopic level, it can be seen that the modes of failure are quite unique. It is evident that film L7 fails because the poor coalescence of the film at the interparticle boundaries results in regions too weak to support the stress. Individual particles pulled out of the uncoalesced matrix are quite distinct in Figure 8(b) and (c). This failure mechanism is logical, considering the nature of the virgin film [Fig. 5(g)]. The film contains voids resulting from film shrinkage on drying where cracks can easily initiate, followed by failure in the poorly fused interstitial regions.

The remainder of the materials exhibited intermediate fracture energies for brittle failure, and much higher energies for ductile failure. Figures 9 and 10 show the micrographs of both failure modes for the two optimum materials, L3 and L5, respectively.

Figure 9(a) is a low magnification view of the brittle crack, and Figure 9(b) a higher magnification view of the steppe regions. Evidently, the crack surface is more complex and has a higher energy than those of L1 and L7, since the crack travels on a multitude of planes, seeking the lowest energy path (0.037 J mm^{-2}). The remaining micrographs in Figure 9 depict a ductile fracture surface of another specimen prepared from the same material. The micrograph in Figure 9(c) shows the overall surface, while (d) and (e) are successively higher magnifications. The intricate, multidirectional pathway followed by the crack and the difficulty of the crack fronts to merge accounts for the high energy to break (0.55 J mm^{-2}). Failure still occurs in the boundary regions, as revealed by careful study of Figure 9(e).

Polymer L5 also exhibited superior properties. Micrographs of ductile and brittle failure are shown in Figure 10. The specimen depicted in Figure 10(a), (b), and (c) was a brittle break (0.035 J mm^{-2}). The microstructure of the surface is similar to that of the other brittle failures. In contrast, Figure 10(d) and (e) correspond to ductile failure (0.35 J mm^{-2}) of a different specimen. As with L4, the crack follows both horizontal and vertical tortuous pathways in an attempt to minimize fracture energy. The crack is deflected to the weak regions presented by the partially fused interfaces, resulting in multiplanar crack propagation. It should be noted that the fusion levels for the intermediate modulus materials are higher than those for the highly crosslinked materials (L6 and L7), accounting for the superior performance in both failure modes.

CONCLUSIONS

High speed tensile testing followed by fractograph examination indicated that both the bulk material properties and the degree of particle coalescence determines the strength of cast latex films.

Latexes that contain an excess of chain transfer agent are completely fused (as shown by SEM) and it is postulated that the poor properties result from insufficient entanglement of the polymer chains. SEM showed that films cast from latexes synthesized with an excess of crosslinking agent were poorly fused, and had correspondingly low energies to break. Cracks moved easily through both the low molecular weight and the highly crosslinked polymers. Yet, the failure mechanisms for the two materials were distinctly different. The former produced fresh homogeneous surfaces when broken that

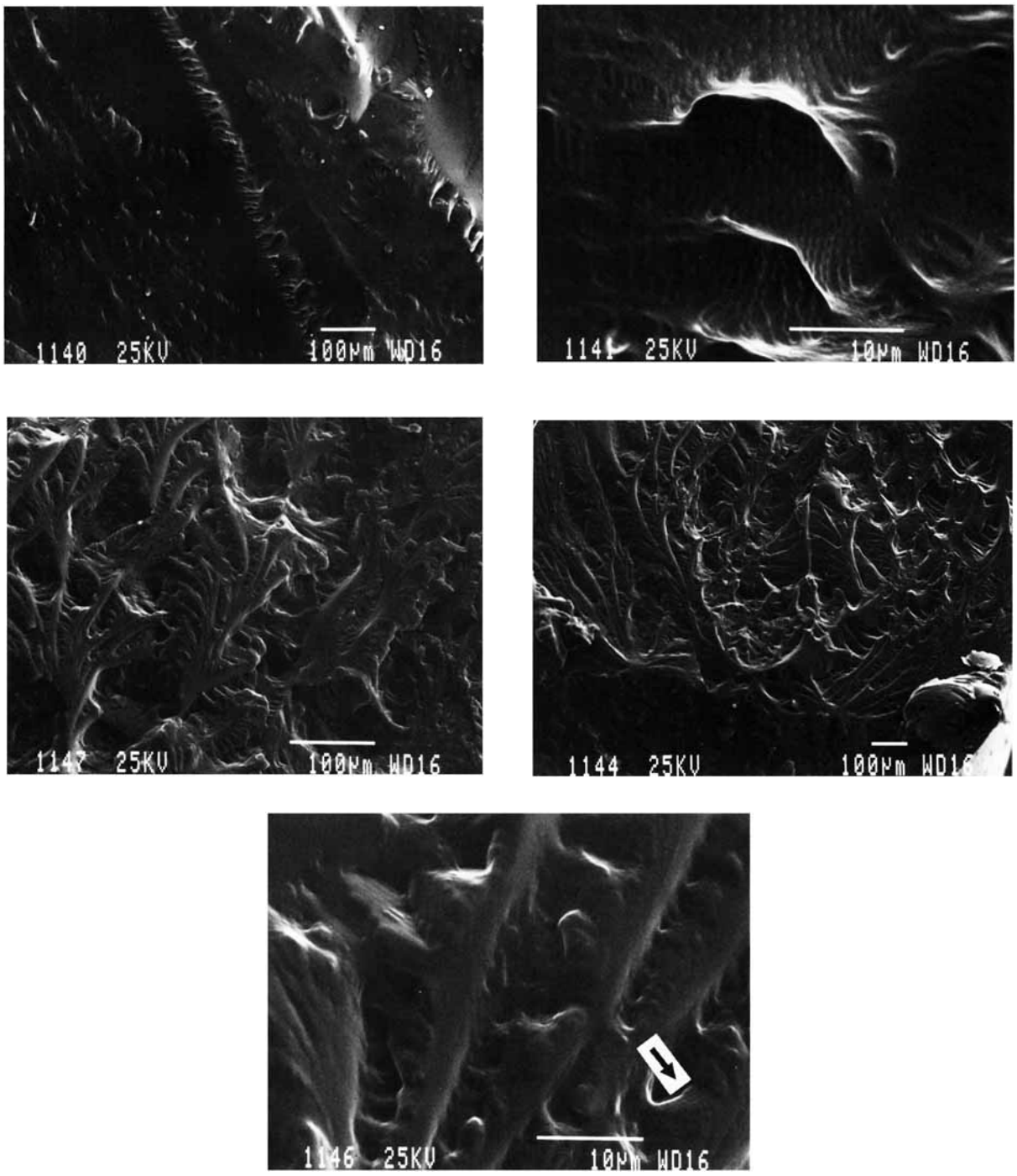

Figure 9 Scanning electron micrographs of fracture surface, Film L3.

appeared identical to the as-cast film. The latter fractured at the unfused particle interfaces.

Materials containing intermediate levels of molecular weight modifiers exhibited superior behavior. Both the peak force at break and the fracture energy were significantly improved. Fractography revealed that although fracture occurred in the partially fused regions, multiplanar crack propagation yielded higher fracture energies.

The results indicate that an optimum emulsion polymerization formulation exists that produces a polymer that is lightly crosslinked, yet still capable of forming a partially fused nascent film. Although the coatings were evaluated at a high strain rate, it

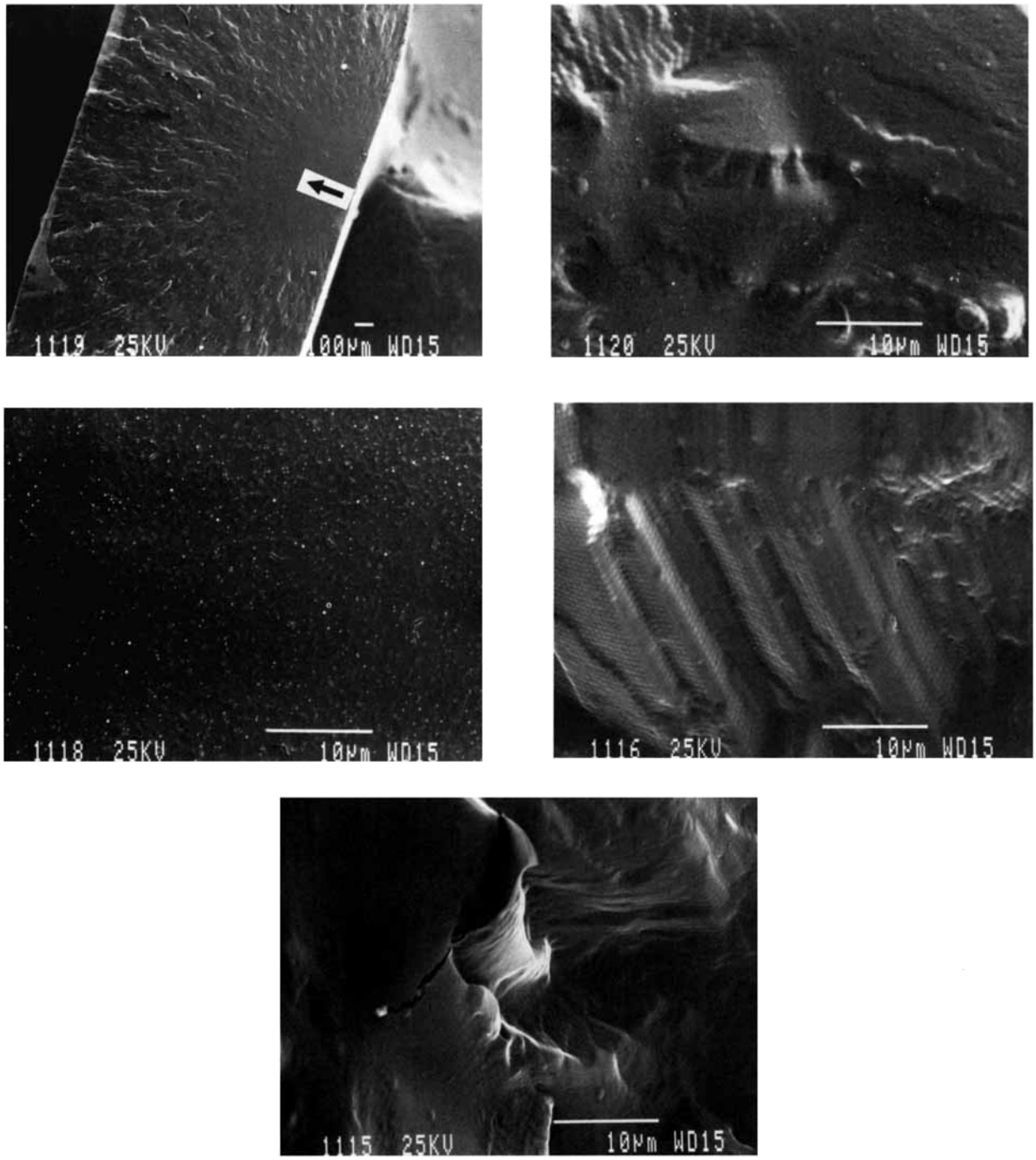

Figure 10 Scanning electron micrographs of fracture surface, Film L5.

is likely that the same trends would be observed at the lower strain rates typical of normal usage conditions.

This research was supported by the Natural Sciences and Engineering Research Council of Canada. The authors wish to thank Dr. David Cook for his assistance with the data analysis.

APPENDIX A CALCULATION OF THE FRACTURE ENERGY

The energy to break (or fracture energy) is calculated using the following expression:

$$E_b = \frac{A_{rc} g v}{A l_c}$$

E_b = fracture energy per unit area (J mm^{-2})
A_{rc} = area under raw data curve (mV s^{-1})
g = gravitational acceleration (m s^{-2})
v = jaw speed (m s^{-1})
A = crossectional area of specimen (mm^{-2})
l_c = load constant (mV kg^{-1})

APPENDIX B
CALCULATION OF PEAK FORCE AT BREAK

The peak force at break is calculated using the following equation:

$$F = \frac{pg}{A l_c 10^6}$$

F = peak force at break per unit area (MPa)
p = peak voltage from raw data trace [see Figs. 5(a) and 5(b)] (mV)
g = gravitational acceleration (m s^{-2})
l_c = load constant (mV kg^{-1})
A = crossectional area of specimen (m^{-2})

REFERENCES

1. W. Doll, in *Fractography and Failure Mechanisms of Polymers and Composites*, chap. 10, A. C. Roulin-Moloney, ed., Elsevier Applied Science, Essex, U.K., 1989.
2. P. Fenelon, *Poly. Eng. Sci.*, **15,** 538 (1975).
3. R. Ecker, *Rubber Chem. Tech.*, **39,** 823 (1966).
4. A. Kobayashi and N. Ohtani, *J. Appl. Polym. Sci.*, **16,** 2523 (1972).
5. M. Yokouchi, S. Seto, and Y. Kobayashi, *J. Appl. Polym. Sci.*, **28,** 2209 (1983).
6. S. S. Voyutskii, *J. Polym. Sci.*, **32,** 528 (1958).
7. K. Hahn, G. Ley, H. Schuller, and R. Oberthur, *Colloid. Polym. Sci.*, **264,** 1092 (1986).
8. K. Hahn, G. Ley, and R. Oberthur, *Colloid. Polym. Sci.*, **266,** 631 (1988).
9. M. A. Linne, A. Klein, L. H. Sperling, and G. D. Wignall, *J. Macromol. Sci.-Phys.*, **B27(2&3),** 181 (1988).
10. M. A. Linne, A. Klein, G. A. Miller, L. H. Sperling, and G. D. Wignall, *J. Macromol. Sci.-Phys.*, **B27(2&3),** 217 (1988).
11. J. N. Yoo, L. H. Sperling, C. J. Glinka, and A. Klein, *Macromolecules*, **23,** 3962 (1990).
12. C. L. Zhao, Y. Wang, Z. Hruska, and M. A. Winnik, *Macromolecules*, **23,** 4082 (1990).
13. M. J. Devon, T. Provder, and A. Rudin, *ACS Symp. Serv.*, **472,** 135 (1991).
14. D. G. Cook, A. Plumtree, and A. Rudin, *Polym. Sci. Eng.*, **30,** 596 (1990).
15. B. H. Bersted, *J. Appl. Polym. Sci.*, **24,** 37 (1979).
16. F. Bueche and T. J. Dudek, *Rubber Chem. Tech.*, **36,** 1 (1963).

Received June 10, 1992
Accepted August 26, 1992